Finite Element Analysis of Structural Steel Impact Damage and Heat Straightening

Norman Fong, MSc. Candidate

University of Waterloo

Waterloo, Canada

Robert Gracie, Ph. D

University of Waterloo

Waterloo, Canada

Scott Walbridge, Ph. D

University of Waterloo

Waterloo, Canada

Abstract

Damage to overpassing bridges commonly occurs due to corrosion, fatigue, and vehicle impact. Unlike corrosion and fatigue, where damage develops slowly over time, impact damage due to over-height vehicles is sudden and unpredictable. This paper briefly introduces the heat straightening process and reviews cases where heat straightening for bridge remediation after vehicle impact was found to be cost-effective. In addition, this paper presents several Finite Element Analysis (FEA) studies performed to determine the required level of complexity to model structural steel impact damage and heat straightening for the purpose of structural assessment and remediation design. The impact studies focus on comparing the residual stresses, strains, and displacements for two common methods of analysis, i.e.: *quasi-static* and *dynamic* analysis. The heating process for heat straightening repairs is simulated using a simplified modelling approach and the results are compared to experimental plastic rotation data at different heating temperatures. Heat straightening parameters such as heating time, support conditions, and heating method are then discussed. With the proposed method for modelling the heating process, the motion and heat from the torch are represented with multiple segments and heating convection coefficients. The results from the simplified FEA for impact and heat straightening are used to discuss the validity of the modelling techniques and assumptions used. Further work is needed to apply the investigated analysis methods to full-scale bridge girders. Experimental study is also recommended to obtain material parameters and further validate the analysis methods.

1.0   Introduction

Heat straightening is a method of repairing steel girders that have been subjected to impacts from over-height vehicles. Impacts on steel bridge girders by over-height vehicles occur frequently, due to inattentive drivers or a misjudgement of bridge clearance. Heat straightening uses multiple cycles of heat applied in specific patterns to remediate deformed steel girders. In many situations, heat straightening repairs can be economic and disruptions to traffic are lower [1], [2].

Heat straightening repair is often a viable economic alternative to a full-girder replacement with lower traffic disruptions. The Lees Avenue Underpass in Ottawa, Canada and the Brockhampton Bridge in the United Kingdom are examples of successful heat straightening applications. Minimization of traffic disruption was preferred because both bridges were in high traffic locations. Heat straightening of the Lees Avenue Underpass was completed in 20 nights whereas the full-girder replacement would have required 60 days to complete. Heat straightening resulted in cost savings for the Lees Avenue Underpass and Brockhampton Bridge of $1.43 million [2] and $660,000 (£360,000) [1] respectively.

Heat straightening originated from techniques used to camber steel beams. The earliest records of heat straightening can be traced to the 1930s [3]. The use of heat straightening was limited initially to experienced practitioners. Up until the 1980s structural repairs using heat straightening were limited in the US in many states [3]. These restrictions were due to limited understanding and quantification of the process, parameters, and effects of heat straightening on steel. Restrictions were removed when a comprehensive heat straightening guide was created for the US Federal Highways Administration (FHWA) addressing these concerns. "The Guide for Heat straightening of Damaged Steel Bridge Members" detailed techniques and recommendations for the heat straightening process.

Heat straightening is the process of applying cycles of heat in specific patterns with small jacking forces to slowly deform steel sections. Elevated temperatures in the heated regions soften the steel. The unheated regions restrain the softened steel from longitudinal thermal expansion, limiting the steel to expand laterally. The longitudinal contractions that occur during the cooling phase are greater than the expansion that occurs during heating. The FHWA recommends that temperatures during heat straightening be limited to 650°C because they can be misperceived by ±56°C. Steel temperatures during heat straightening exceeding 700°C start approaching the lower critical temperature of steel, where phase changes occur. Phase changes in steel may lead to changes in ductility and yield strength that negatively affect the bridges performance. Jacking forces may not cause stresses exceeding 50% of the yield strength because the yield strength is reduced up to 50% at elevated temperatures. Common patterns used in heat straightening include: vee, line, strip, and spot heating [3].

The current paper focuses on vee heat straightening, which is used to straighten a member along the strong axis. Oxyacetylene torches are used to elevate the temperatures in the heated area following a specific pattern, as shown in Figure 1. Progressing from the tip of the triangle to the base, the heat from the torch increases the temperature of the heated region to a relatively uniform level. The heated region will contract more at the base than the tip during cooling, causing the steel member to bend. Each heat straightening cycle deforms the plate a fraction of a millimetre. Heat straightening results are often measured in terms of plastic rotation. Plastic rotation (∅) is the longitudinal angular change caused by heat straightening, measured in milliradians (mrad), as shown in Figure 1.
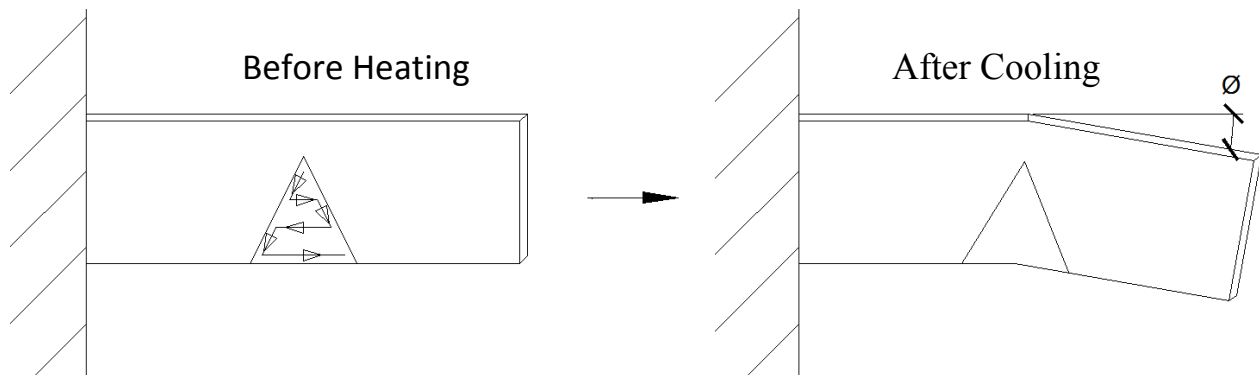
Figure 1: Schematic look at vee heat straightening of a plate.

Finite Element Analysis (FEA) can be used to investigate the deformations and the residual stresses in a girder after impact and heat straightening. FEA is used in the automotive industry to model hot-forming processes and crashworthiness of car parts, for example [4]. Additional constitutive model parameters are required to incorporate the strain-rate and temperature dependence of the plastic behaviour of steel during impact and forming processes. Similar FEA-based simulation techniques can also be applied to the modelling of impact damage and heat straightening of bridge elements.

2.0   Description of Research Procedures and Objectives

Heat-straightened bridge girders are subjected to plastic deformation from vehicle impacts and repairs using heat straightening. The objective of the work presented herein is to explore the effects of impact and methods of modelling heat straightening using FEA. Deformed bridge girders can be complex and

shapes may vary depending on the impact. Two-dimensional plate girder sections and plate elements are used herein to simplify the analysis of impact and heat straightening, respectively.

Effects of impact are compared using different modelling techniques involving quasi-static and dynamic analysis. The material model used in the FEA includes the strain-hardening and strain-rate sensitivity properties of steel. The results focus on different impacts categorized by mass, speed, and displacement using a controlled impactor and two-dimensional plate girder section. These impacts are compared using residual stress, strains, and displacements from the steel section.

Heat straightening of girders is a complex procedure. Steel girders are composed of multiple plate elements. The study of heat straightening was simplified in the current study by focusing on single plate elements heated using the vee heat straightening method. Vee heat straightening relies on temperature-control, jacking forces, vee geometry, and support conditions. The current study examines aspects of the application of heat and support conditions that affect heat straightening. The results are compared to experimental plastic rotation and temperature data in the literature [5].

The following sections include descriptions of the finite element models and material properties used to explore the various methods of modelling impact damage and heat straightening. The support conditions, elements, parameters used to model impact damage and heat straightening are discussed. The material properties assumed for each model are presented in separate sections of the paper. The FEA was performed using the commercially available ABAQUS software.

2.1   Finite Element Model for Impact Damage Modelling

For the impact damage modelling, an I-section with a flange thickness of 25 mm and width of 100 mm was used. The I-section web was 10 mm thick and 200 mm deep. The purpose of the analysis was to model a possible bench-scale test involving a projectile impacting the web at the mid-height. A rigid 25 mm diameter impactor of varying mass and velocity was assumed to strike the web as shown in Figure 2. The impactor movement was limited to horizontal displacement. The mid-height of the I-section was restrained from vertical displacement to model a plane of symmetry and the sides of the flanges were restrained from moving horizontally. 6.35 mm fillet welds were modelled. Clearly the modelled impact scenario has significant differences compared with an actual bridge girder impact.
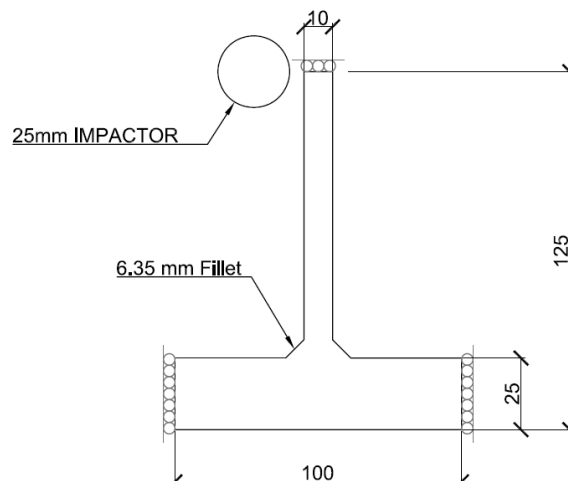
Figure 2: Boundary conditions and dimensions for an I-section subjected to an impact from a circular projectile.

4

The model geometry was discretized using 4-node bilinear plane-strain elements. The projectile was assumed to be rigid and its surface was discretized using 2-node elements. The moment of inertia of the impactor was assumed to be 20,431 mm^4 with its center of mass at its center.

Quasi-static and dynamic analysis are two common methods used to model impact. Quasi-static analysis simulates an impact at a rate where inertial and strain-rate effects are negligible, whereas dynamic analysis accounts for both inertial and strain-rate effects. The impact in the quasi-static analysis was controlled by slowly moving the impactor to deform the web. The impactor slowly depressed the web between 10 mm and 40 mm, the deformed shape was measured after the impactor load was removed. The dynamic analysis impacts were controlled by specifying the initial mass and velocity of the impactor. The dynamic analyses assumed impactor masses of 20 g/mm, 30 g/mm, and 40 g/mm and velocities of 17 m/s, 25 m/s, and 34 m/s or approximately 60 km/h, 90 km/h, and 120 km/h, respectively.

Residual stress, plastic strain, and displacement results were compared between quasi-static and dynamic experiments with similar deformed shapes. Results were limited to impacts where the final deformed shape had a web displacement greater than 8 mm, based on [6].

2.2   Material Properties for Impact Damage Modelling

The modelled material was 350W steel. The elasticity was described using general properties of steel; the plasticity was characterized with plastic stress-strain data for CSA 350W steel. Effects from strain-rate were calculated using the Cowper-Symonds equation. The density of steel, Young's modulus, and Poisson's ratio were 7.85 g/cm^3, 200 GPa and 0.3, respectively. The plastic stress-strain response of CSA 350W steel was obtained from tensile specimen data from a coupon of a W310x39 wide flange [7]. Figure 3 shows the plastic true stress-strain curve starting at the 416 MPa, where the steel starts to yield; the data in the figure extends up to a plastic true strain of 1 using a power-law fit.
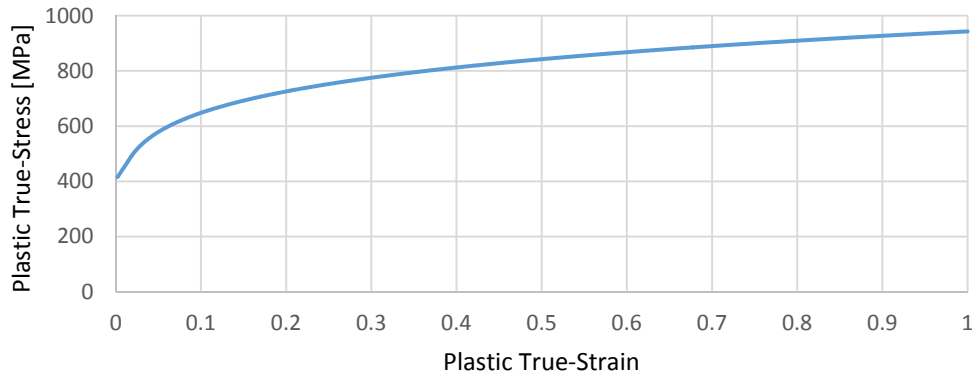
Figure 3: CSA 350W assumed plastic true stress-strain curve.

The Cowper-Symonds equation relates static yield stress to dynamic yield stress and it is commonly used for strain-rate sensitive materials. Equation 1 shows this relationship where the dynamic yield stress (σ') and static yield stress (σ_0) is related to strain rate ($\dot{\epsilon}$) using the parameters D and q:

$$\frac{\sigma'}{\sigma_0} = 1 + \left(\frac{\dot{\epsilon}}{D}\right)^{\frac{1}{q}} \qquad (1)$$

Cooper-Symonds parameter D and q values of 6844 s^{-1} and 3.91 in this study, due to the high plastic strains that occur during impact, these values are appropriate for mild steel behaviour closer to ultimate tensile stress [8]. Figure 4 shows dynamic yield strength factors relative to the strain rate using the Cowper-Symonds Relationship. At a strain rate of 0.001 s^{-1}, the static yield strength increases by a factor of 1.02 whereas a strain rate of 1000 s^{-1} increases static yield strength by 1.61. As a result, the yield strength of the steel will be dependent on the strain rate it experiences during impact.

$$\frac{\sigma'}{\sigma_0} = 1 + \left(\frac{\dot{\epsilon}}{D}\right)^{\frac{1}{q}}$$
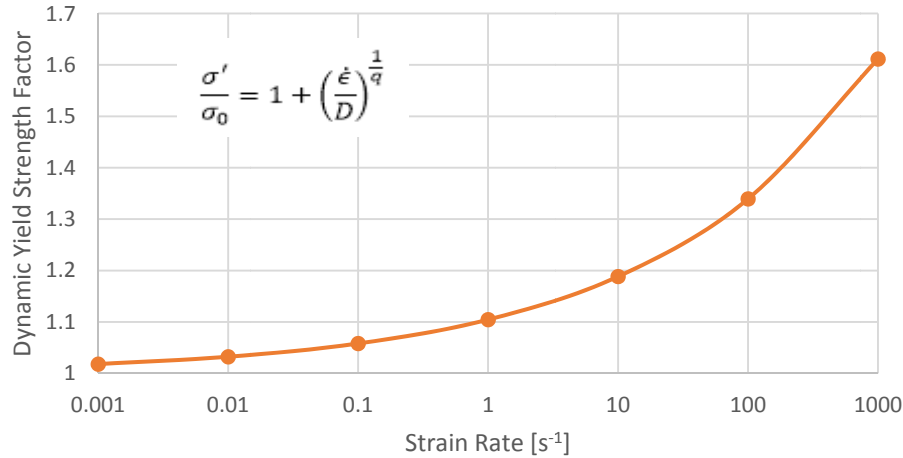
Figure 4: Dynamic yield stress factor versus strain rate using Cowper-Symonds relationship.

2.3   Modelling of Heat Straightening

Implicit coupled temperature-displacement analysis was used to model heat straightening of undamaged steel plates using vee heat straightening. To model heat straightening, a nonlinear calculation that simultaneously solves for displacements and temperatures is needed. Temperature-Displacement Octahedral (C3D8T) elements were used to discretize simple, undamaged plates for this analysis. All of the plates modelled were 6 mm thick x 100 mm wide with an unsupported length of 610 mm as shown in Figure 5. Each plate was subjected to ¾ depth 60° vee heat with jacking forces applied against the base of the heated triangular section. Two support conditions shown in Figure 5 were studied: fixed-fixed and pin-pin, where both ends are fixed and pinned, respectively

Out-of-plane deformation was restrained at the top and bottom sides of the plate. Jacking forces were applied to create the flexural jacking ratio of 0.16 used in experiments from [5] on similar plate specimens. The flexural jacking ratio is a function of the jacking moment over the plastic moment capacity of the section. Additional restraints were placed at the pin-pin supports.

Convection and radiation boundary conditions were defined on the surfaces of the plate and only changed for surfaces subjected to heat. The ambient temperature was set to 25°C for surfaces where heat was not directly applied. A cooling convection coefficient of 7.9 W/mm^{2}K and an emissivity of 0.8 were assumed. Heat transfer using radiation requires emissivity and the Stefan-Boltzmann coefficient. The emissivity is highly dependent on the condition of the steel plates; recently milled plates and oxidized plates have an emissivity of 0.3 and 0.8 respectively, according to [9]. The Stefan–Boltzmann coefficient was taken as 5.67 x 10^{-2} W/m^{2}K^4 and used for the cooling radiation equation.
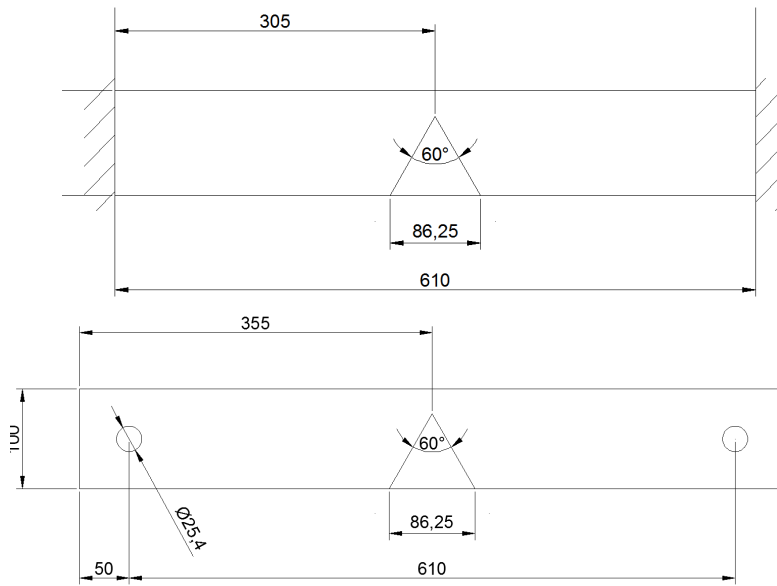
Figure 5: Tested support conditions for 6x100 mm wide plates during heat straightening.

The motion and heat from an oxyacetylene torch during the heat straightening process was simplified as a set of strips and heat transferred using convection. The convection load sequentially heated strips from the tip to the base of the vee to emulate the meandering motion of the torch; the heated strips divided the heated region as shown in Figure 6. The temperature of an oxyacetylene flame was assumed to be 3250°C during heating and the application of heat was controlled by convection coefficients. Sets of convection coefficients were adjusted so each strip reached 621°C and each strip was heated for equal periods of time. These times were varied and compared with plastic rotations for 60° vee patterns from the test data at various temperatures. The maximum temperature of each strip was measured and averaged for each plastic rotation. Heating times may vary in reality and are dependent on field conditions, plate thickness, torch settings, and technician experience. These heating times were used to investigate the effect of heating time on the straightening process. The goal of this modelling method was to develop a simplified approach for modelling heat straightening in practice.
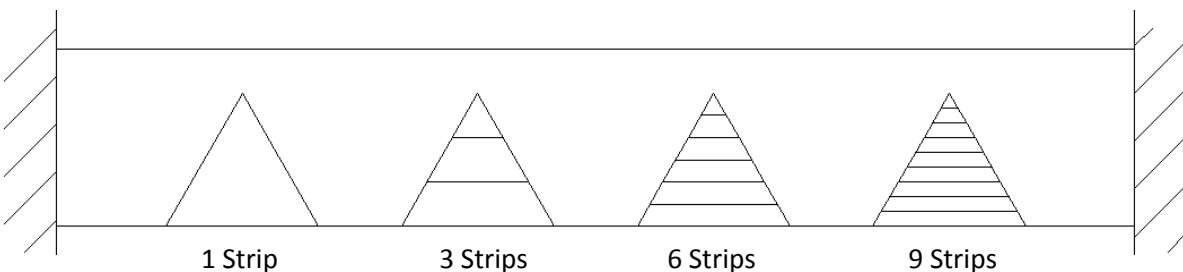
Figure 6: Segmentation of heated vee pattern into strips.

7

The results of analyses performed with various boundary condition assumptions and heating sequences are compared with the experimental data from [5]. To facilitate this comparison, plastic rotations and surface temperatures reported in this reference are compared with the model predictions.

2.4   Material Properties for Modelling of Heat Straightening

The experimental data from [5] was based on tests performed on used A36 steel. This material was modelled using general properties for mild steel, plastic stress-strain data for A36 steel, and thermal properties for steel from the European structural fire codes. The density, Young's modulus, and Poisson's ratio were taken as 7.85 g/cm^3, 200 GPa, and 0.3. The following thermal properties of mild steel (see Figures 7 to 10) were assumed, based on the European structural fire codes [12]:

- coefficient of thermal expansion,
- specific heat,
- thermal conductivity,
- Young's modulus reduction factors, and
- yield strength reduction factors.

The assumed plastic stress-strain behaviour of the A36 is shown in Figure 11, based on [13].
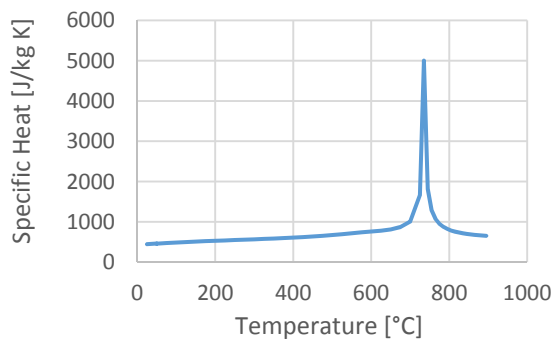
Figure 7: Specific heat of mild steel versus temperature.
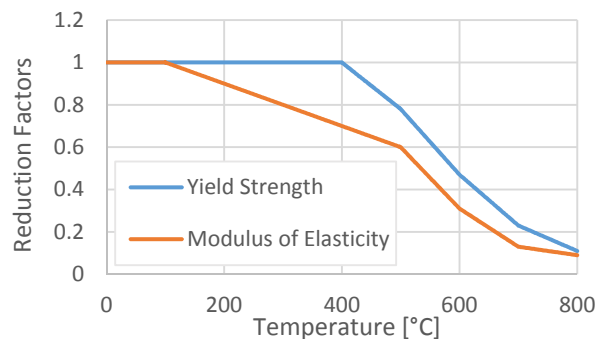
Figure 8: Reduction factors for yield strength and modulus of elasticity relative to temperature.
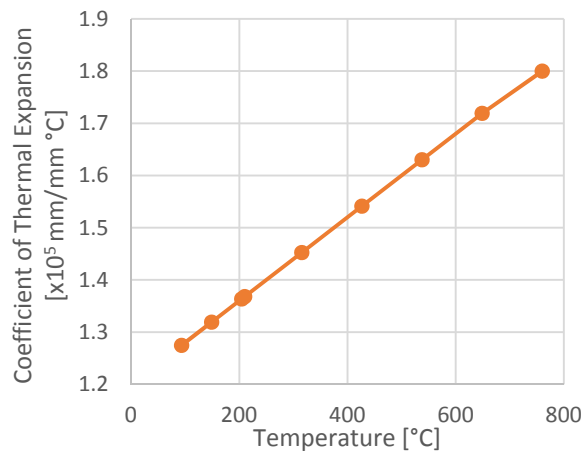
Figure 9: Coefficient of thermal expansion of mild steel relative to temperature.
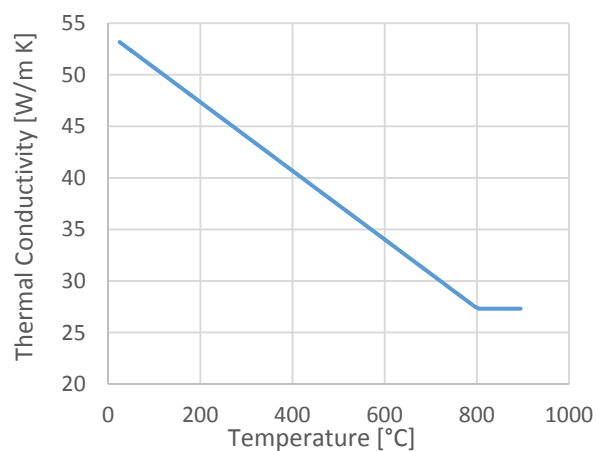
Figure 10: Thermal conductivity of mild steel versus temperature.

8
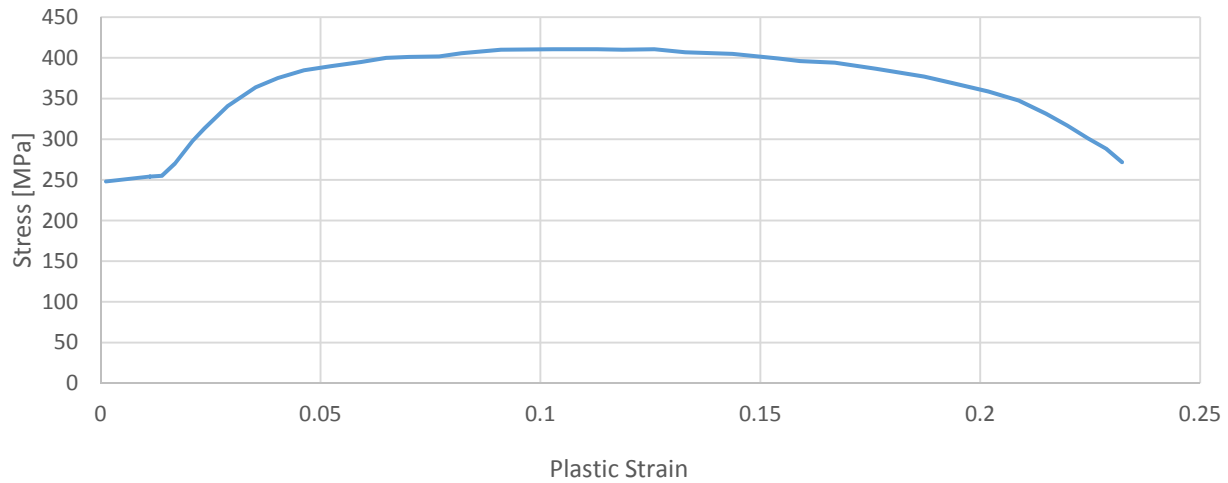
Figure 11: Plastic stress-strain curve of A36 steel [13].

3.0 Finite Element Analysis Results

The following section contains results from the impact damage and heat straightening studies.

3.1 Impact Model Results

The I-section was subjected to 15 different impact analyses, with parameters such as impact velocity varied; residual stress and strain was compared for impacts resulting in similar deformed shapes. The residual stress, strain, and final displacements through are reported along two paths, as shown in Figure 12 below: Path 1 is along the web surface and Path 2 is through web thickness. Results from Path 1 and 2 were considered locations of interest where high concentrations of stress and strain occurs.
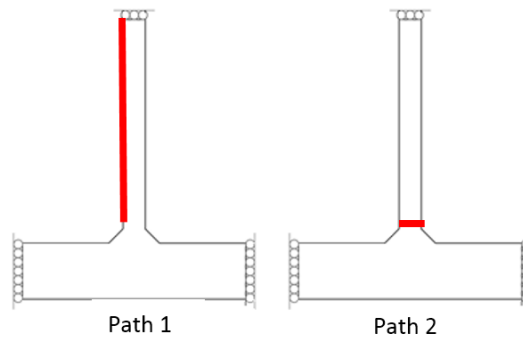
Figure 12: Measurement paths for results of impact damage study.

In the following figures, the following convention to identify the analysis results is assumed: **x mm** indicates that the result was from an **x** mm displacement-controlled impact, and **yy g-zz** refers to a result for an impactor mass of **yy** grams/millimetre travelling at a velocity of **zz** m/s.

Figure 13 shows the final displaced shape of the I-section measured along Path 1 for several quasi-static and dynamic impact analyses, focusing on analyses that resulted in similar final displacements. The

10

15 mm quasi-static analysis (for example) caused a similar deformation to the dynamic analysis for the 20 g and 40 g impactors with velocities of 25 m/s and 17 m/s, respectively. (Note: the imactor weights are small in this analysis, since the FE model is a 2D model with a thickness of 1 mm.)

Figure 14 indicates similar strain levels along the majority of the web face for these three cases. The strains from the quasi-static analysis were higher than those from dynamic analysis and occurred at the point of impact and base of the web where strain-rate is high. The majority of the elevated strains were within the first 20 millimetres of the base of the web and from the point of impact.
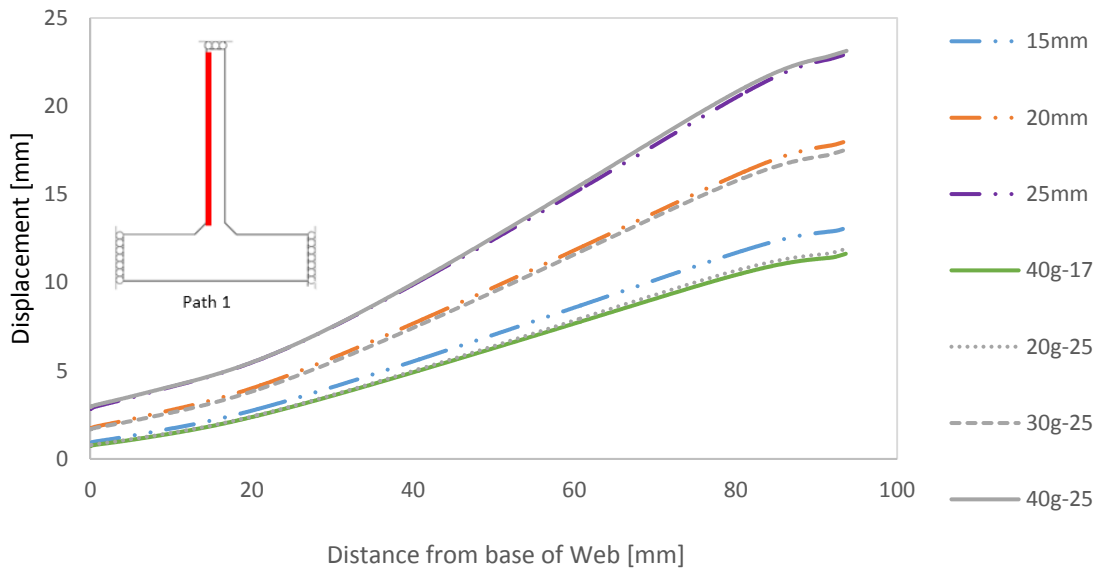
Figure 13: Final displacement along Path 1 for quasi-static and dynamic experiments with similar displacements.
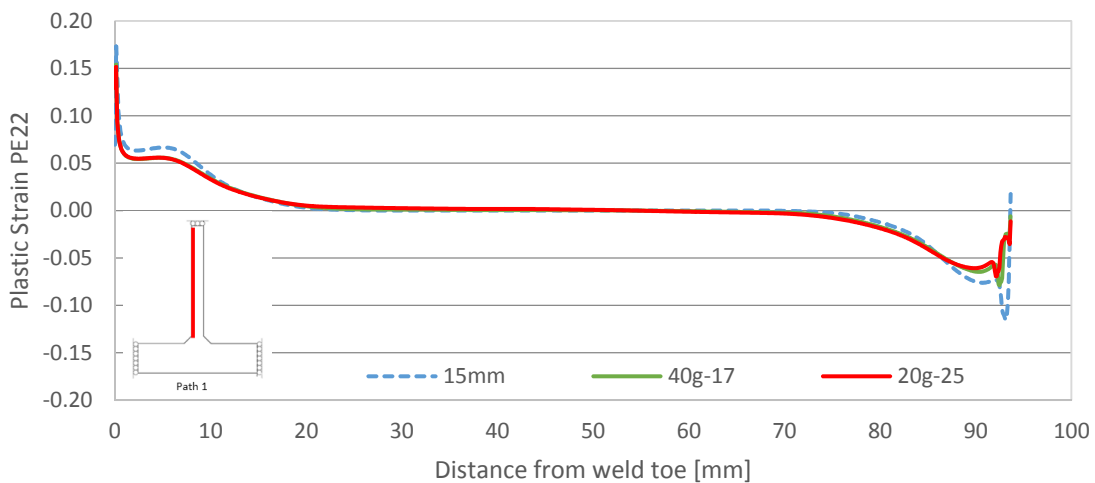
Figure 14: Plastic Strain PE22 along Path 1 for 15 mm, 20g-25, and 40g-17 experiments.

Regions of higher strain should also have higher stresses. Figure 15 shows bending stress S22 along Path 1 for the three selected impacts. Unlike the plastic strain PE22, the distribution of residual stress S22 caused by the quasi-static and dynamic impacts varies significantly throughout. Differences in stress are

caused by different strain rates from each impact. The 20g/m impactor resulted in a lower residual stress magnitude at the weld toe (distance = 0 mm) than the 40g/m dynamic experiment. The highest residual stress magnitude at the weld toe was seen in the quasi-static analysis, -761 MPa, whereas the residual stresses in the dynamic analyses were -477 MPa and -186 MPa for the 17 m/s and 25 m/s analyses, respectively. Faster impact velocities appear to relate to a lower residual stress magnitude at the weld toe. Figure 16 shows the residual stress S22 along Path 2 for the same 15 mm (quasi-static), 20g-25, and 40g-17 analyses. The residual stresses along Path 2 differed within 1-2 mm of the surfaces on either side of the web. In particular, the dynamic impact analyses caused significantly lower residual stress magnitudes than the quasi-static analysis on either surface in comparison with the dynamic analyses. Stress reversals could have been caused by the springback at the end of impact.
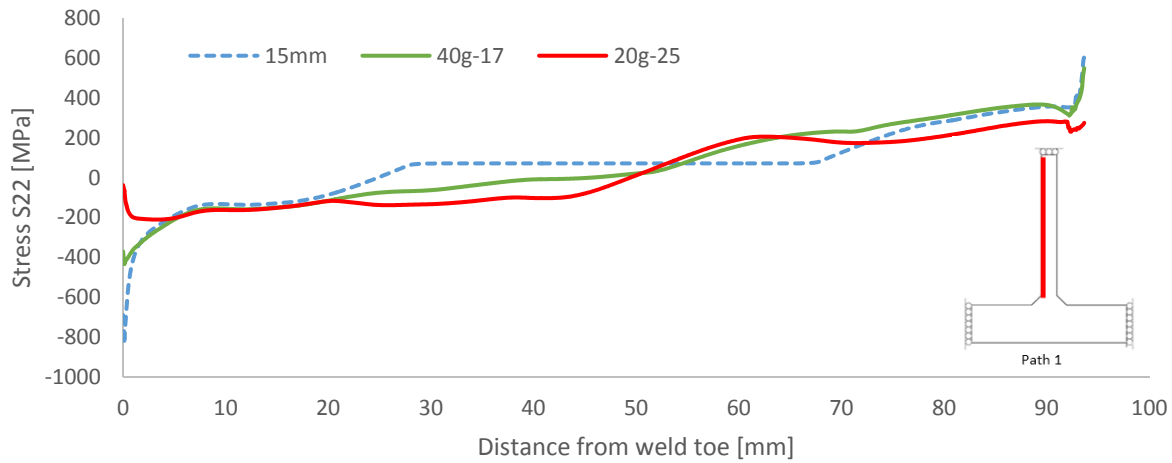
Figure 15: Stress S22 along Path 1 for 15 mm, 20g-25, and 40g-17 experiments.
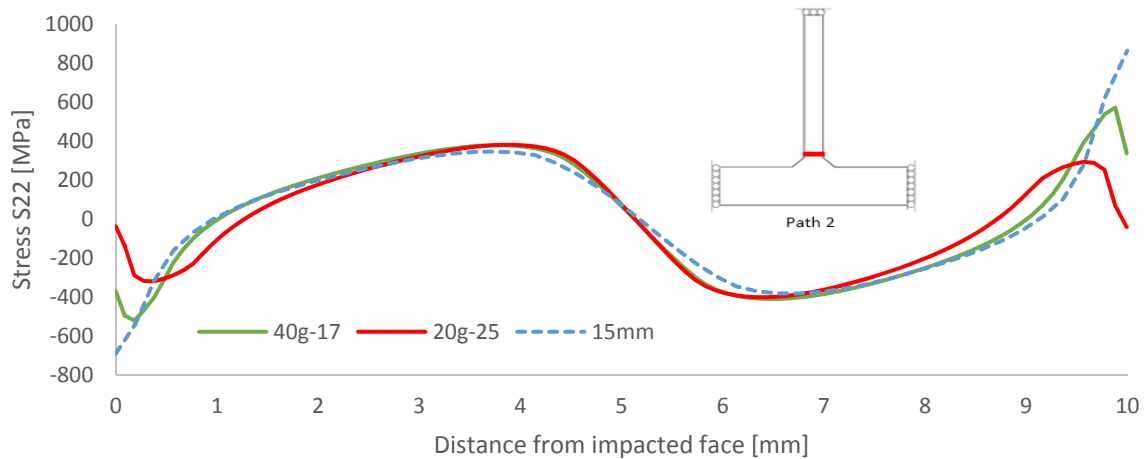
Figure 16: Stress S22 along Path 2 for 15 mm, 20g-25, and 40g-17 experiments.

3.2   Heat Straightening Analysis Results

Plastic rotations at different temperatures were used to compare the effects of various support conditions, heating methods, and heating times on the heat straightening analysis. Plastic rotations from

FEA were compared to experimental data for straight plates deformed using vee-heat straightening [5]. The average maximum temperature used in this section refers to the average of maximum temperature in each strip measured when the strip is heated; each strip is a segment of a heated area. Results where the ends are pinned and fixed were compared at various temperatures. Experimental plastic rotation is compared to FEA results where the plates were assumed to have fixed ends and the heating method was varied from 1 strip to 9 strips. The effect of heating times on heat straightening are examined by comparing results where plates were heated to 621°C at two different rates.

Temperature control is difficult and temperatures in the field can be misinterpreted by up to ±56°C [5]. The average maximum temperature refers to the temperature at the end of each heating step. The FEA results show up to a 46°C temperature drop after 1 second of cooling. After heating 3 strips in 3 minutes to 629°C, the temperature proceeded to drop to 583°C after 1 second of cooling. Any delays in measurement could explain the 56°C misinterpretation of temperature.

Figure 17 shows that heat straightening analysis results for fixed-fixed and pin-pin support conditions at various "maximum" temperatures (e.g. temperatures at the end of the heating period). Results between the two support conditions are similar. However, the observed maximum temperatures (e.g. after 1 second of cooling) were closer between the two support conditions.

Figure 18 shows plastic rotation results for all versions of the heat straightening FEA model at different maximum temperatures with different heating methods and times (for the fixed-fixed case). The plates heated in 3 strips with different heating times had up to a 45°C difference in temperature to achieve similar plastic rotations. However, average temperature during the heating process remained similar with a difference of ±2°C in most cases. The results from the two different rates of heating steel showed the effect of heating time on the heat straightening analysis results. Effectively doubling the heating time of a plate resulted in a relatively small (50°C) decrease in maximum temperature.
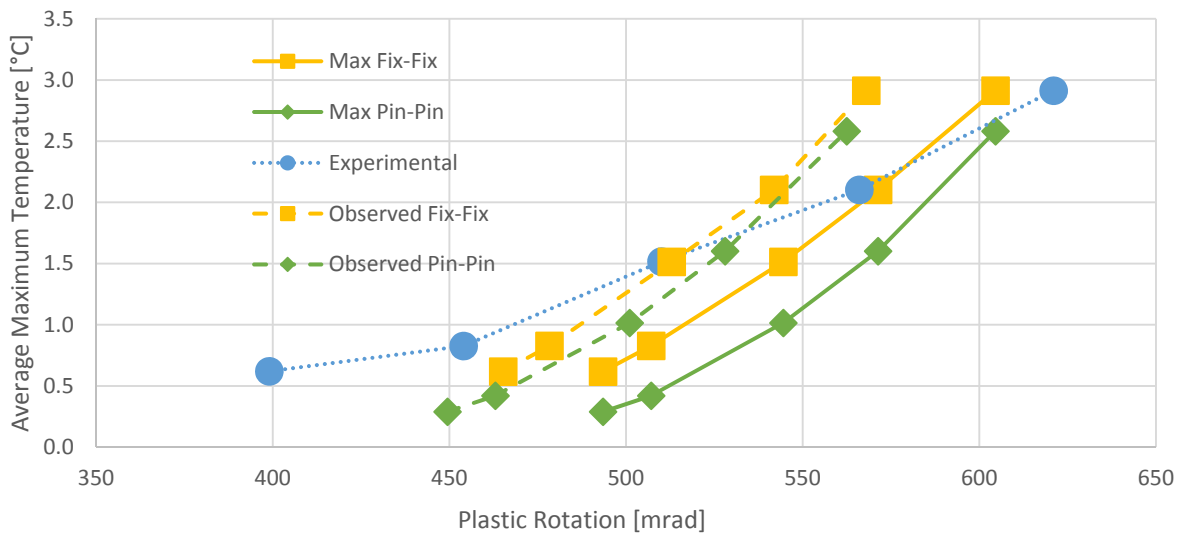
Figure 17: Plastic rotations for fixed-fixed and pin-pin support conditions at different maximum temperatures.
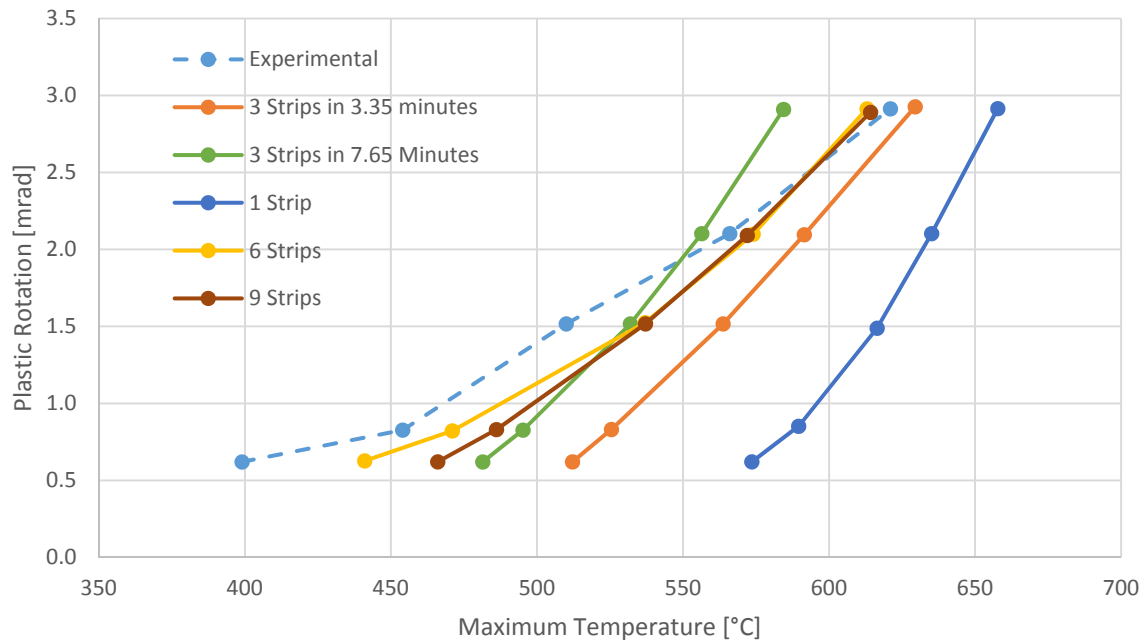
Figure 18: **Plastic rotation versus maximum temperature of different heating schemes (fixed-fixed).**

Heating the triangular vee area as one strip or area was significantly less effective than heating the area with multiple strips. It requires an additional 29°C to 64°C to reach similar plastic rotations by heating the area in 1 strip compared to 3 strips where both were heated in a similar time. The increase in plastic rotation from the experimental data and FEA results between 450°C and 621°C appears almost linear. Each set of FEA heat straightening results show that heat straightening is less effective at lower temperatures. Heating the area sequentially with an increasing number of multiple strips reduced the temperature differences between the FEA results and the experimental data. Presumably the use of more strips more closely models the actual heating process, where a torch is moved along a path to heat the vee region locally rather than heating the whole vee region uniformly.

4.0   Conclusions

4.1   Impact Damage Analysis

Residual stresses due to impact damage may be lower than predicted in a quasi-static analysis. Using a quasi-static analysis to recreate a deformed shape (e.g. based on measurements in the field) may not yield accurate results because this approach doesn't account for the strain rates that occur during impact. Higher velocity impacts in the analyses presented herein resulted in lower residual stresses; the high-velocity impacts caused higher strain-rates where the steel yield strength was increased as a function of strain-rate based on the Cowper-Symonds equation. Further research is recommended to extend this finding to 3D analysis of full-scale bridge girders. Additional lab experiments are also recommended to verify the strain-rate sensitivity of CSA 350W steel. The Cowper-Symonds relationship should be calibrated for this particular steel grade and set of strain rates.

4.2　Heat Straightening Analysis

Effective vee heat straightening depends on the manner in which the heat is introduced, including the heating rate of steel and the progression of heat (i.e. heating path). The rate of heating was not seen to be a large factor when the rate is sufficiently slow to heat the plate through the thickness. Approximately doubling the time to heat a plate resulted in a ~50°C decrease in maximum temperature for comparable plastic rotations. These FEA results with different rates of heating steel validate previous observations that the time required to heat a plate has a minute effect [5].

Temperature control and measurement in the field is difficult and it is possible to misjudge the temperature by ±56°C. This error can be justified by any delays in measurement, the FEA results showed that elevated temperatures dropped up to 46°C temperature after one second of cooling. It is possible for differences in temperature between experimental and FEA results to be explained by delays in measurement. In most cases, the differences in temperature were less than 50°C.

The method of heat application often described for vee-heat straightening requires elevating the temperature of the region slowly from the tip of the vee to the base. The simplified process of progressively heating strips can be a comparable way of modelling the heating process in FEA. Increasing the number of strips reduced the differences between the experimental data and FEA results. This simplified heating process with multiple strips was less effective in predicting the experimental results at lower temperatures. The effect of heat straightening was highly dependent on the maximum surface temperature where a 50°C increase could result in a ~0.5 milliradian increase in plastic rotation.

An investigation into heat straightening at lower and higher temperatures compared to experimental data is required. Further research into alternatives to simulating the heating process used is in progress. Results should be extended to comparison with other vee angles used in heat straightening.

Bibliography

[1]　S. K. Clubley, S. N. Winter and K. W. Turner, "Heat-straightening repairs to a steel road bridge," *Bridge Engineering,* no. BEI, pp. 35-42, 2006.

[2]　Ontario Ministry of Transportation, "Heat Straightening of Lees Avenue Underpass Girder," *RoadTalk,* no. Spring 2012, 2012.

[3]　US Federal Highway Administration, "Guide for Heat-Straightening of Damaged Steel Bridge Members," US Federal Highway Administration, 2008.

[4]　Oasys Software house of Arup, "LS-Dyna," [Online]. Available: http://www.oasys-software.com/dyna/en/software/ls-dyna.shtml. [Accessed April 2014].

[5]　R. R. Avent, D. J. Mukai, P. F. Robinson and R. J. Boudreaux, "Heat Straightening Damaged Steel Plate Elements," *Journal of Structural Engineering,* vol. 126, no. 7, pp. 747-754, 2000.

[6]　Alberta Transportation, "Repair of Bridge Structural Steel Elements Manual," Government of the province of Alberta, 2004.

[7]　P. Arasaratnam, K. S. Sivakumaran and M. J. Tait, "True Stress-True Strain Models for Structural Steel Elements," *International Scholarly Research Network,* 2011.

[8]   Fire and Blast Information Group, Design Guide for Steels at Elevated Temperatures and High Strain Rates, Ascot: The Steel Construction Institute, 2001, p. 30.

[9]   H. Sadiq, M. B. Wong, J. Tashan, R. Al-Mahaidi and X.-L. Zhao, "Determination of Steel Emissivity for the Temperature Prediction of Structural Steel Members in Fire".

[10] C. W. Roeder, "Experimental Study of Heat Induced Defomation," *Journal of Structural Engineering,* vol. 112, no. 10, pp. 2247-2262, October 1986.

[11] K. J. Kowalkowski and A. H. Varma, "Structural Proerpties of Steels Subjected to Multiple Cycles of Damage Followed by Heating Repair," *Journal of Structural Engineering,* vol. 133, no. 2, pp. 283-296, 2007.

[12] European Committee for Standarisation, EN 1993-1-2: Eurocode 3: Design of steel structures: Part 1-2: General Rules - Structural fire design, CEN, 2005.

[13] R. L. Brokenbrough and B. G. Johnson, Structural Alloys Handbook, vol. 3, 1994, p. 5.